Role of Defect Sites and Ga Polarization in the Magnetism of Mn-Doped GaN

D. J. Keavney,[1] S. H. Cheung,[2] S. T. King,[2] M. Weinert,[2] and L. Li[2]

[1]*Advanced Photon Source, Argonne National Laboratory, Argonne, Illinois 60439, USA*
[2]*Department of Physics, University of Wisconsin, Milwaukee, Wisconsin 53211, USA*

(Received 25 July 2005; published 12 December 2005)

We report a study of the Mn local structure, magnetism, and Ga moments in molecular beam epitaxy grown Mn-doped GaN films. Using x-ray absorption spectroscopy and magnetic circular dichroism, we find two distinct Mn sites and a Ga moment antiparallel to Mn. First-principles calculations reproduce this phenomenology and indicate that Mn preferentially populates Ga sites neighboring N split interstitial defects. These results show that defects may strongly affect the Mn ordering and magnetism, and that the GaN valence band is polarized, providing a long-range ferromagnetic ordering mechanism for $Ga_{1-x}Mn_xN$.

DOI: 10.1103/PhysRevLett.95.257201 PACS numbers: 75.50.Pp, 75.25.+z, 78.70.Dm

Doped magnetic semiconductors have received considerable attention as part of the search for a new class of spintronic devices [1], with a primary goal of realizing a room-temperature ferromagnetic semiconductor [2–5]. In Mn-doped III-V semiconductors, Mn nominally substitutes for the group III atom and simultaneously provides a localized magnetic moment and a hole, leading to Mn $3d$-host $4sp$ exchange and ferromagnetic ordering. Defect sites may also be present, and can play an important role in the distribution of Mn and its magnetic ordering. In GaAs, Mn interstitials strongly affect the Curie temperature T_C and drive its dependence on post deposition annealing through hole compensation. However, the importance of defects, and the types of defects present, will be very much dependent on the host compound, hence what is known about GaAs may not be applicable even to other III-V compounds. Therefore, understanding of magnetism in doped semiconductors requires knowledge of defects and their interactions with the Mn site distribution and the $3d$-$4sp$ exchange.

X-ray absorption spectroscopy (XAS) and x-ray magnetic circular dichroism (XMCD), coupled with theoretical understanding of realistic defect-induced band structures, offer a way to resolve these issues. Recently Wu [6] compared calculated XAS and XMCD spectra in $Ga_{1-x}Mn_xAs$ with experimental data [7,8], and showed that the inclusion of Mn interstitial sites and substitutional-interstitial dimers can have a strong effect on the spectra. In addition, XMCD can detect induced moments at the group III and V sites, indicating how the host participates in the magnetic ordering [8].

Mn-doped GaN may offer the promise to go beyond cryogenic Curie temperatures. Theoretical work predicts T_C well above 300 K [9,10], and experimental T_C from 10 to 900 K have been reported [11,12]. Manganese is expected to occupy Ga sites as a $2+$ ion, and Edmonds *et al.* [13] recently reported Mn $L_{3,2}$ x-ray absorption on molecular beam epitaxy (MBE) grown $Ga_{1-x}Mn_xN$, confirming the divalent state. However, d^4 and d^3 configurations have also been detected using other methods and under varying growth and codoping conditions [14,15], raising the possibility of variations of the electronic structure due to defects that could be causing the observed T_C variations. Epitaxial GaN films are known for very high defect densities, and the role of these defects and of interstitial Mn in the magnetic ordering is not well known.

In this Letter, we report an XAS and XMCD study of the Mn electronic structure and induced Ga moments in single-phase Mn-doped GaN films with varying Mn concentrations, together with first-principles calculations for a variety of defects. We find that the XAS and XMCD data, including the observed small antiparallel Ga moment, can be explained consistently if Mn is preferentially bound to N split interstitials. Our results also suggest interstitial Mn does not exist in significant quantities in these samples.

The $Ga_{1-x}Mn_xN$ films were grown on 6H-SiC (0001) substrates by electron-cyclotron resonance plasma-assisted MBE [16]. The 60 nm GaN buffer layer was grown at 570 °C. The subsequent 150 nm Mn-doped layers were grown at 500 °C and with the addition of H_2 to the nitrogen plasma, which is found to suppress the formation of precipitates [16]. Four films, 150 nm thick, were grown with Mn doping, x, of 1.5, 1.9, 3.6, and 4.5%, as determined by Mn/Ga peak ratio in energy dispersive spectroscopy. A pseudo (1×1) surface reconstruction was observed by reflection high-energy electron diffraction (RHEED) on the buffer layer, suggesting 2D growth and a Ga-terminated polar surface [17]. For the Mn-doped layer, spotty RHEED patterns indicate 3-dimensional under nitrogen rich conditions [16].

The XAS and XMCD measurements were taken at beam line 4-ID-C of the Advanced Photon Source [18]. The samples were mounted in a superconducting solenoid with the field along the x-ray beam propagation direction, with the beam at 20° above the film plane. The beam line resolution at the Mn L edge was set to ~0.27 eV. Data were collected in total electron yield by monitoring the sample photocurrent. The photon polarization was re-

 © 2005 The American Physical Society

versed at each energy point in a fixed field of up to 5 T. The Ga L edge XMCD measurements were repeated with fields of opposite sign to rule out the presence of artifacts.

The first-principles spin-polarized local density approximation (LSDA) electronic structure calculations used the full-potential linearized augmented plane wave (FLAPW) method [19] as implemented in *flair*. The defect calculations used cells with 32 or 96 atoms, and included full structural relaxation. All calculations were done at the theoretical lattice constants ($a = 3.18$ A, $c/a = 1.6256$; the corresponding experimental values are $a = 3.19$ A and $c/a = 1.627$). For the defects calculations, there was one Mn in the given defect configuration per supercell. Thus, for a nominal 32-atom $2 \times 2 \times 2$ supercell, the Mn concentration (relative to Ga) is $1/16 = 6\%$, while the 96 atom cells correspond to $\sim 2\%$ Mn concentration. The Mn XAS and XMCD spectra were modeled by the unoccupied $3d$ and $4s$ local density of states (DOS) [20]. The calculations did not assume any charge state for the Mn, but rather calculate the electronic structure self-consistently. To account for some final state effects, calculations in the presence of Mn $2p_{3/2}$ ($m_j = \pm 3/2$) core holes ("final state rule") were done for selected cases. Using the DOS as an approximation to the XAS spectra neglects multiplet effects except to the extent that the LSDA approximately projects out M_J states out of the full multiplets.

In Fig. 1, we plot the Mn $L_{3,2}$ edge absorption (upper curves) and dichroism (lower curves) data for four samples ranging from $x = 1.5$ to 4.5%. The L_3 edge is split into two components, indicated as A and B, with peak positions separated by ~ 0.7 eV. For $x = 4.5\%$, we show a comparison with a calculated XAS spectrum (dotted line) based on a simple two-site Mn^{2+} atomic multiplet model with a fixed energy shift of 0.7 eV between the two spectra [21]. The major features present in the calculated spectrum are also present in the data, and the line positions are well reproduced. This multicomponent spectrum suggests that two structurally inequivalent Mn sites are present. Both of these components contribute to the dichroic signal in all samples, indicating that neither is due to a simple oxide contamination, as is sometimes the case for $Ga_{1-x}Mn_xAs$ [8,22–24]. Another possibility is a ferromagnetic secondary phase; however, extensive structural characterization shows no evidence for precipitates. Cross-sectional transmission electron micrographs taken on similar samples show no inclusions at nanometer length scales, and x-ray photoemission electron microscopy rules out larger-scale Mn-rich inclusions. The doping dependence of the relative populations of these two sites (Fig. 1 inset), shows that while both spectral features increase in intensity with doping, occupation of site B becomes more likely at higher Mn concentrations. Models including 3+ and 4+ multiplets resulted in unsatisfactory fits, thus we conclude only Mn^{2+} is present.

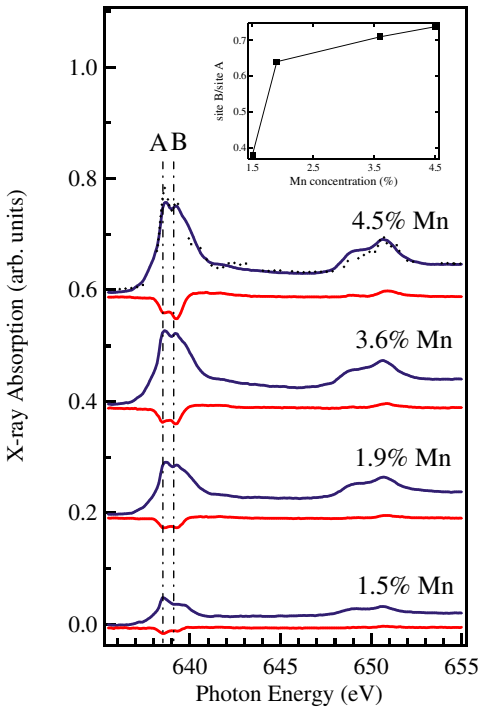

FIG. 1 (color online). X-ray absorption spectroscopy (blue curves) and magnetic circular dichroism (red curves) at the Mn $L_{3,2}$ edges for each Mn concentration, taken at 4.2 K in a +2 T field. Feature A on the primary L_3 peak is consistent with the Mn^{2+} calculation. The intensity of feature B, ~ 0.7 eV above A, scales with Mn doping. The dotted curve superimposed on the 4.5% XAS is a two-site Mn $3d^5$ high spin atomic calculation with no crystal field splitting. Inset: doping dependence of the ratio of the intensities of the two features.

The temperature dependence of the XMCD signal of each feature for the $x = 1.5$ and 3.6% samples (main panel) and the Curie temperature associated with feature B for all four samples (inset) are shown in Fig. 2. Clearly, the ordering temperature of this phase is highly dependent on the Mn doping, with films containing more than 3.6% Mn exhibiting T_C greater than 300 K. This would not be expected from clusters of a magnetic minority phase, but it is entirely consistent with ordering in a homogeneously doped magnetic semiconductor. Therefore, this is further evidence that the explanation for the multicomponent spectrum in these films is two inequivalent Mn^{2+} sites intrinsic to $Ga_{1-x}Mn_xN$ grown under N-rich conditions, and not a precipitate phase.

We find an XMCD signal at the Ga L_3 edge which increases with Mn doping. In Fig. 3, we show the XAS and XMCD taken in a +5 T field at 4.2 K from an additional sample with 3.0% Mn. The bipolar line shape is similar to that seen in $Ga_{1-x}Mn_xAs$ [8], as is the position of the features at the onset of the absorption edge, placing the spin-polarized states they arise from close to the Fermi level. An estimate of the area under the XMCD curve (dashed line) based on a fit to two Gaussians of opposite

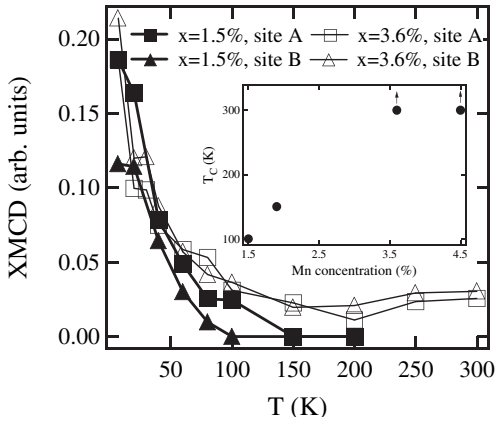

FIG. 2. Temperature dependence of the XMCD intensity for the two features in the 1.5 and 3.6% Mn samples. Inset: doping dependence of the Curie temperature associated with feature B, derived from the XMCD data. Arrows above the two highest Mn concentration points indicate that the Curie temperature is above 300 K, the highest temperature for which XMCD was measured.

sign indicates a net Ga polarization. Taking into account the sign change due to the selection rules between $3d$ and $4s$ dichroism [25], we find a Ga moment that is *antiparallel* to the Mn moment, which is the opposite spin configuration from $Ga_{1-x}Mn_xAs$ [8] and recent predictions for $Ga_{1-x}Mn_xN$ [26].

To understand the nature of the two Mn sites and the antiparallel alignment of the Ga, first-principles calculations of substitutional Mn_{Ga} neighboring an array of possible defect sites were considered. For GaN grown under N-rich conditions, split interstitials, where an N site contains 2 N atoms [27], are more favorable than simple N interstitials, and are therefore included. In Fig. 4(a), the calculated (ground state) Mn L_3 absorption spectra are given [20]. Simple Mn_{Ga} substitutions and the single and double Mn near a N split interstitial most closely reproduce the observed Mn^{2+} line shape, while all other types of defects result in line shapes qualitatively inconsistent with the XAS and/or XMCD data. In particular, interstitial Mn (Mn_I) results in a shift of $\sim$2 eV below the main line for Mn_{Ga}; this would result in pre-edge structure which is not observed. The spectrum for substitutional Mn_{Ga} has a two-peaked structure in the DOS, separated by $\sim$0.7 eV; since the minority DOS is the dominant contribution to both the XAS and XMCD spectra, they have similar shapes. Even though this peak separation is similar to the experimental data, simple Mn_{Ga} alone cannot account for the experimental results since the relative intensity of the two peaks changes with Mn concentration, and these sites result in a parallel Ga moment ($\sim 0.02\mu_B$/Ga). Only the N split interstitial configurations result in antiparallel Ga ($\sim 0.03\mu_B$/Ga) and N ($\sim 0.06\mu_B$/N) moments. Thus, under N-rich growth conditions, Mn occupies Ga sites neighboring N split interstitials, and there is little effect of Mn interstitials on its magnetic properties in GaMnN.

The energetics favor the formation of Mn-N split interstitials: the total energy difference between the combined Mn-N split interstitial complex and the separated N split interstitial and Mn_{Ga} defects is 2.54 eV for the Mn in the basal plane, as shown in the upper left corner of Fig. 4. Mn

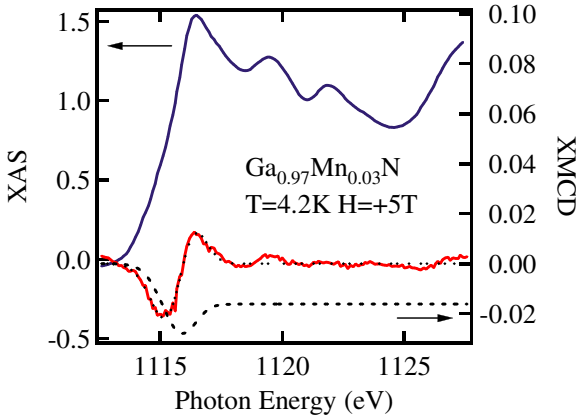

FIG. 3 (color online). XAS (blue) and XMCD (red) at the Ga L_3 edge in a +5 T field at 4.2 K. The sign of the initial dichroism suggests a Ga moment that is antiparallel to the Mn $3d$ moments. The dashed line is an estimate of the area under the XMCD curve based on a fit (dotted line) to two Gaussians of opposite sign.

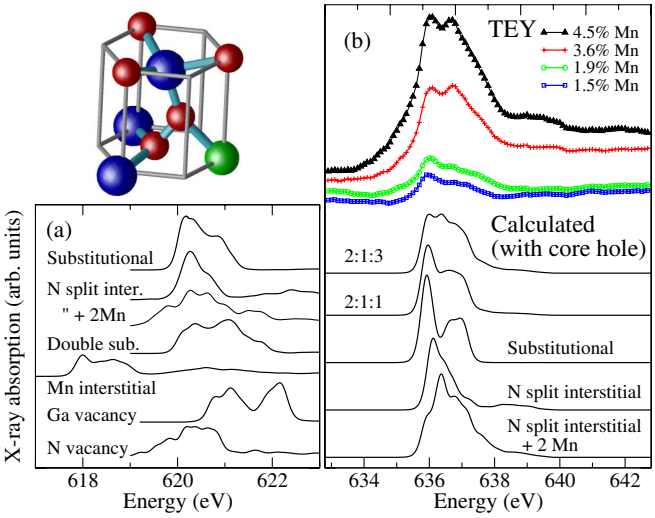

FIG. 4 (color online). Upper left: calculated local structure of a Mn (green) atom next to an N (red) split interstitial defect. (Ga atoms are in blue.) (a) Ground state unoccupied Mn DOS for different defects. (b) Experimental XAS spectra (colored) for different Mn concentrations, compared to calculations in the presence of core holes for substitutional Mn_{Ga}, for one and two Mn atoms next to a N split interstitial (bottom three spectra), and for different superpositions of these spectra (top two calculated). The energy scale is set using total energy differences, and the experimental spectra are shifted to match the most intense L_3 peaks with the simple Mn_{Ga} calculation. The spectra for the substitutional and N split interstitial defects were calculated using 96 atom cells; all others used 32 atom cells.

in the "top" site is ~0.6 eV less bound. The binding energy (1.05 eV) of a second Mn (at the top site), although smaller than the binding of the first Mn, is still significant. (With the second Mn also in the basal plane, the binding is reduced by ~0.3 eV.) The moments of the two Mn atoms are preferentially antiferromagnetically coupled (by ~0.04 eV), with a moment of $\sim 3.5\mu_B$ for the basal plane Mn and about $-1.8\mu_B$ for the top Mn, leading to a net magnetic moment for the complex.

The calculated Mn XAS spectra in the presence of a core hole for substitutional Mn_{Ga} and N split interstitial defects are shown in Fig. 4(b). (The differences in the spectra for the ferro- and antiferromagnetically coupled Mn atoms next to an N split interstitial are minor.) Based on these results, we attribute feature *A* in the experimental data to substitutional Mn_{Ga} and feature *B* to a combination of Mn (both single and multiple Mn atoms) next to N split interstitials and Mn_{Ga}. The calculated energy difference between Mn_{Ga} and two Mn atoms next to an N split interstitial is ~0.5 eV, slightly smaller than the observed splitting, but consistent with the experimental data. The two upper calculated spectra in Fig. 4(b) are the composite of the calculated spectra for substitutional, N split interstitial, and N split interstitial plus two Mn in the ratio as indicated. These two spectra clearly show the effect of increasing N split interstitials: the high-energy peak grows in relative intensity, and there is a narrowing of the peak separation, consistent with the experimental observations.

This behavior for GaN differs from that in GaAs, where Mn_I-Mn_{Ga} dimers appear to be important [6]. The significantly smaller volume of GaN leaves little room for Mn interstitials, whereas the larger atomic size of As greatly hinders the formation of As split interstitials. Thus, the principal defects in the two materials are intrinsically different, but in both cases will affect the Mn distributions and magnetic properties.

The picture that emerges is that for N-rich growth the Mn will preferentially bind to N split interstitials at higher Mn concentrations. The Mn site populations will depend on both the concentration of Mn and N split interstitials and the diffusivity of Mn. As the Mn concentration increases, the probability of a Mn and an N split interstitial being within a diffusion length increases, leading to an increase in the number of Mn-N split interstitial complexes relative to isolated Mn_{Ga} and an increase in feature *B*. Since the Ga moment is antiparallel to the Mn across the entire composition range that we studied, this argues that a large fraction of Mn_{Ga} sites neighbor N split interstitials. Since the relative importance of N split interstitials will depend on their density, the conditions during sample growth will have an influence on the effects we report. This offers a potential explanation for the variations in magnetic properties reported in the literature, as well as differences with previous x-ray absorption results [13]. Finally, the net magnetic moment on Ga demonstrates that the valence band of GaN is polarized, providing a long-range ferromagnetic ordering mechanism for $Ga_{1-x}Mn_xN$.

Work at UWM was supported by the National Science Foundation (DMR-0094105). Use of the Advanced Photon Source was supported by the U.S. Department of Energy, Office of Science, under Contract No. W-31-109-Eng-38.

[1] H. Ohno, Science **281**, 951 (1998).
[2] Y. Ohno *et al.*, Nature (London) **402**, 790 (1999).
[3] M. Tanaka and Y. Higo, Phys. Rev. Lett. **87**, 026602 (2001).
[4] E. Johnston-Halperin *et al.*, Phys. Rev. B **65**, 041306(R) (2002).
[5] K. C. Ku *et al.*, Appl. Phys. Lett. **82**, 2302 (2003).
[6] R. Wu, Phys. Rev. Lett. **94**, 207201 (2005).
[7] D. Wu *et al.*, Phys. Rev. B **71**, 153310 (2005).
[8] D. J. Keavney *et al.*, Phys. Rev. Lett. **91**, 187203 (2003).
[9] T. Dietl *et al.*, Science **287**, 1019 (2000).
[10] K. Sato, P. H. Dederics, and H. Katayama-Yoshida, Europhys. Lett. **61**, 403 (2003).
[11] G. T. Thaler *et al.*, Appl. Phys. Lett. **80**, 3964 (2002).
[12] S. Sonoda *et al.*, J. Cryst. Growth **237-239**, 1358 (2002).
[13] K. W. Edmonds *et al.*, J. Appl. Phys. **95**, 7166 (2004).
[14] T. Graf *et al.*, Appl. Phys. Lett. **81**, 5159 (2002).
[15] B. Han, B. W. Wessels, and M. P. Ulmer, Appl. Phys. Lett. **86**, 042505 (2005).
[16] Y. Cui and L. Li, Appl. Phys. Lett. **80**, 4139 (2002).
[17] A. R. Smith *et al.*, Appl. Phys. Lett. **72**, 2114 (1998).
[18] J. W. Freeland *et al.*, Rev. Sci. Instrum. **73**, 1408 (2002).
[19] E. Wimmer, H. Krakauer, M. Weinert, and A. J. Freeman, Phys. Rev. B **24**, 864 (1981); M. Weinert, E. Wimmer, and A. J. Freeman, Phys. Rev. B **26**, 4571 (1982).
[20] The spatial localization of the local DOS is determined by the overlap of the valence states with the Mn $2p_{3/2}$ core states. The calculated spectra are broadened by the derivative of the Fermi distribution, $\sim \mathrm{sech}^2(E/2E_0)$, with $E_0 = 0.075$ eV. For ground state spectra, the energies are given relative to the Mn $2p_{3/2}$ eigenvalues; for excited state (core-hole) spectra, the energy scales of the unoccupied DOS are determined by the difference in total energies between calculations of the ground state and one with a core hole. The ~16 eV shift between the ground state and the core-hole spectra results mainly from the fact that the eigenvalues are only one contribution to the (Koopman's) electron removal energies, neglecting the incomplete cancellation of the Coulomb self-interaction, and do not include final state effects.
[21] G. van der Laan and B. T. Thole, Phys. Rev. B **43**, 13 401 (1991).
[22] K. W. Edmonds *et al.*, J. Appl. Phys. **95**, 7166 (2004).
[23] H. Ohldag *et al.*, Appl. Phys. Lett. **76**, 2928 (2000).
[24] Y. Ishiwata *et al.*, Phys. Rev. B **65**, 233201 (2002).
[25] S. S. Dhesi *et al.*, Phys. Rev. B **60**, 12 852 (1999).
[26] E. Kulatov *et al.*, Phys. Rev. B **66**, 045203 (2002).
[27] S. Limpijumnong and C. G. Van de Walle, Phys. Rev. B **69**, 035207 (2004).